The Astronomical Journal, 166:117 (6pp), 2023 September https://doi.org/10.3847/1538-3881/ace7b8

Understanding the Capability of Future Direct-imaging Observations to Quantify Atmospheric Chemical Effects of Stellar Proton Events

Georgios P. Afentakis[1,7], Kyla Mullaney[2,7], Howard Chen[3,4], John Blalack[2], Jade Checlair[5], and Dorian S. Abbot[6]
[1] Department of Physics, University of Chicago, Chicago, IL, USA; gpafentakis@uchicago.edu
[2] Department of Astrophysics, University of Chicago, Chicago, IL, USA
[3] Planetary Environments Laboratory, NASA Goddard Space Flight Center, Greenbelt, MD, USA
[4] Department of Aerospace, Physics, and Space Sciences, Florida Institute of Technology, Melbourne, FL, USA
[5] Boston Consulting Group, Toronto, Canada
[6] Department of the Geophysical Sciences, University of Chicago, Chicago, IL, USA
Received 2022 December 16; revised 2023 July 5; accepted 2023 July 13; published 2023 August 18

Abstract

Models developed for Earth are often applied in exoplanet contexts. Validation in extraterrestrial settings can provide an important test of model realism and increase our confidence in model predictions. NASA's upcoming space-based IROUV telescope will provide unprecedented opportunities to perform such tests. Here, we use the Planetary Spectrum Generator to simulate IROUV reflected-light spectroscopic observations of flare-driven photochemical changes produced by the Whole Atmosphere Community Climate Model, part of the Community Earth System Model framework. We find that NO_2 is the most observable gas to target, and integrating the signal for two days following the flare and comparing to a baseline of preflare data would achieve the highest signal-to-noise ratio. The NO_2 response is much larger for K-star tidally locked planets than G-star rapidly rotating planets and does not depend strongly on O_2 level. The NO_2 response should be observable for planets within 3–4 pc independent of the phase angle since the amount of reflected light is larger at smaller phases, but the NO_2 concentration is low near the substellar point. This work outlines a methodology for validating and ground-truthing atmospheric chemistry models developed for Earth that could be useful for the numerical exploration of exoplanets.

Unified Astronomy Thesaurus concepts: Exoplanet atmospheres (487); Exoplanet atmospheric composition (2021); Direct imaging (387); Radiative transfer simulations (1967); Radiative transfer (1335)

1. Introduction

Atmospheric chemistry and photochemistry are important factors in understanding exoplanetary habitability and performing atmospheric retrievals. Photochemical modeling of rocky exoplanets was first performed in one-dimensional (1D) models (e.g., Segura et al. 2005; Kaltenegger & Sasselov 2009; Segura et al. 2010; Hu et al. 2012; Grenfell et al. 2013; Gao et al. 2015; Kozakis et al. 2018) that provided key insights into the effects of stellar spectral energy distribution, stellar variability, and stellar flares. More recently, such modeling efforts have been expanded to the 2D and 3D regimes, usually with atmospheric chemistry and photochemistry as additional subcomponents in global Earth system or general circulation models (Chen et al. 2018, 2019, 2021; Braam et al. 2022; Cooke et al. 2022; Ridgway et al. 2023; Tsai et al. 2022). While the efficiency of single-column models allows one to explore a large parameter space of planetary characteristics, higher dimensional (2D/3D) models are able to simulate the complex interplay among atmospheric dynamics, clouds, radiation, and chemistry and hence provide results with enhanced realism.

Upcoming direct-imaging missions of potentially habitable worlds provide an unprecedented opportunity to test model realism and predictions of terrestrial photochemical models in extrasolar settings. Evaluating the effects of stellar flares on modeled atmospheric chemistry against observational measurements is one such promising potential method. For instance, Chen et al. (2021) studied the effect of stellar flares on the atmospheric chemistry of terrestrial planets using the National Center for Atmospheric Research Whole Atmosphere Community Climate Model (WACCM), a well-studied and well-validated terrestrial Earth system model. They found that stellar flares can affect concentrations of NO_x, HO_x, and O_3, but did not simulate reflected-light observations to determine whether these changes are potentially observable.

The Planetary Spectrum Generator (PSG; Villanueva et al. 2018) is a radiative transfer model that can can simulate spectral observations by current and future telescopes. PSG has been used to simulate both transit spectroscopy (Fauchez et al. 2019; Komacek et al. 2020; Suissa & Wolf 2020; Haqq-Misra et al. 2022) and reflected-light spectroscopy (Checlair et al. 2021; Kopparapu et al. 2021) for terrestrial planets. In the case of reflected-light spectroscopy, PSG parameters can be chosen to simulate a space telescope that may not launch for decades. PSG provides us with the capability to determine whether the changes in atmospheric chemistry due to stellar flares are potentially observable.

In this paper, we use PSG to simulate reflected-light spectral observations of the response of the atmospheric chemistry of a terrestrial planet to stellar flares as simulated by Chen et al. (2021). We assume a 6 m LUVOIR-like telescope as a proxy for NASA's IROUV telescope that will be capable of directly imaging Earth-like planets (National Research Council 2021). We find that NO_2 yields the largest signal-to-noise ratios of any

[7] Co-first author.

simulated molecule, and that changes in NO_2 could be observable for planets within 3–4 pc. Detections would be possible for planets orbiting K stars, regardless of their background oxygen concentration, but not for planets orbiting G stars. The K-star planets simulated by Chen et al. (2021) are tidally locked and they found that their NO_2 concentration is lower near the substellar point than the antistellar point. As a result, we find that the signal-to-noise ratio (S/N) is relatively insensitive to phase. This paper is organized as follows: in Section 2 we describe our methodology and in Section 3 we give our results. We discuss our results in Section 4 and conclude in Section 5.

2. Methodology

We examine the observational implications of flare-induced chemistry on high-mean molecular weight atmospheres by postprocessing the results of Chen et al. (2021), who simulated O_2-rich and O_2-poor atmospheres for planets orbiting both G and K stars. We do not analyze the M-star cases because these planets are likely to fall within the inner working angle of a direct-imaging telescope. The planets have a modern Earth continental configuration. The G-star cases have a modern Earth rotational period (24 hr) and orbital period (1 yr). The K-star cases are tidally locked in a 1:1 spin:orbit state (rotational and orbital period of 92 Earth days) with the substellar point at the equator and 180° longitude (centered on the Pacific Ocean). The atmospheric surface pressure is 1 bar and we consider two levels of atmospheric oxygenation: (1) O_2-rich (21%, modern Earth-like) and (2) O_2-poor (1%, proterozoic Earth-like). WACCM calculates atmospheric chemistry using the Modules for Ozone and Related Chemical Tracers chemical transport model (Kinnison et al. 2007), which has a network of 217 reactions. The horizontal resolution is $1.^{\circ}8 \times 2.^{\circ}5$ and there are 66 vertical levels with a vertical resolution of 0.5–2 km below the stratopause and roughly half a scale height above the stratopause.

We use the PSG (Villanueva et al. 2018) with the Global Exoplanet Spectra add-on to simulate reflected-light spectroscopic observations of these WACCM simulations. We choose parameters appropriate for the direct-imaging IROUV space telescope proposed in the NASA Decadal Survey (National Research Council 2021), which will directly image Earth-like exoplanets. To approximate IROUV, we use the LUVOIR PSG option with a diameter of 6 m. We use the PSG spatial binning option of 3, corresponding to 3 × 3 (lat x lon) binning. A spatial binning of 3 is the smallest option available in PSG. Our results are not sensitive to this choice. For example, we find that the S/N is only ≈5% lower in a test where we used the maximum binning, so that all spatial variability is averaged out. We use the spectral parameters of the Sun for the G-star case and the spectral parameters of a K6V for K-star case. PSG allows us to specify the phase of the simulated observation, which we vary below.

We calculate the S/N for the retrieval of a molecule in the following way. First we use PSG to calculate the signal and noise, in terms of spectral intensity, in two cases: (case 1) including all molecules and (case 2) including all molecules except the molecule of interest. We then define the signal for the molecule of interest, S_i, as the difference between the spectrum in case 2 and case 1, where the index i refers to wavelength bin. Each signal is associated with a noise, N_i, produced by PSG in case 2 (the noise for case 1 is almost identical). We then integrate the signal and noise over a number of days before the flare (S_{0i} and N_{0i}) and after the flare (S_{fi} and N_{fi}). To integrate the signal we take its algebraic mean, while for the noise we use the formula $\frac{1}{N^2} = \sum_k \frac{1}{N_k^2}$ where k is the day. We then calculate the S/N for the measurement in a given wavelength bin (σ_i) as

$$\sigma_i = \frac{S_{fi} - S_{0i}}{\sqrt{N_{fi}^2 + N_{0i}^2}}. \quad (1)$$

Finally, we combine all wavelength bins using the following formula $\sigma = (\sum_i (\sigma_i)^2)^{\frac{1}{2}}$.

We define a molecule with detectable variability as a molecule whose change in abundance in response to the flare can be detected with an S/N of at least 3. We checked H_2O, CO_2, CH_4, O_3, NO_2, N_2O, and H_2 and found that NO_2 is the only molecule with detectable variability among these. We also note that molecules HNO_3, NO+, HO_2NO, H_2O_2, and NO_3 are produced by WACCM, but are not fully supported by PSG, so we were not able to investigate their detectability.

To validate our methodology, we reproduce the NO_2 S/N versus integration time generated by PSG in 1D configuration shown in Figure 6(b) of Kopparapu et al. (2021). Like Kopparapu et al. (2021), we use LUVOIR with a 15 m diameter for this calculation. Kopparapu et al. (2021) use a modern Earth-like planet, so we use the O_2-rich G-star case from the Chen et al. (2021) simulations. The NO_2 concentration in the two models is similar and we calculate signal-to-noise ratios (S/Ns) that are 10% smaller than Kopparapu et al. (2021) for a given integration time (Figure 1). Given that there are many PSG parameters that Kopparapu et al. (2021) may have chosen to be slightly different from our calculation, we consider this an acceptable validation of our methodology.

3. Results

We do not find detectable variations in NO_2 for the planets orbiting G stars, so we focus on the tidally locked K-star planets in what follows. Figure 2 shows the proton fluence (solar flare activity), NO_2 column, and simulated NO_2 S/N for an Earth-sized, oxygen-rich planet orbiting a K-star that is 2 pc from Earth and observed at a phase of 45°. Large responses in NO_2 follow many flares with the largest of them being at days 58, 171 and 280, all of which lead to detectable signals. Some flares do not cause a large NO_2 enhancement and/or lead to small S/Ns. This is because NO_2 production depends on the presence of other photochemically produced species, such as NO and O_3, which are not always available. Additionally, there are some S/N peaks when we include clouds in the calculation that do not appear to be caused by a flare or increase in column NO_2 abundance, with the most prominent examples occurring on days 85, 107, and 225. We believe this is related to an error that the PUMAS radiation scattering scheme used by PSG returns, "maximum asymmetry has been capped." On days where there is a flare and a resulting S/N, the magnitude of the S/N is similar with and without clouds (Figures 2 and 3), so this issue should not substantially affect our main results.

We next discuss the optimal observing strategy for these detectable NO_2 responses to flares. One important consideration is the amount of expensive telescope time necessary to make an observation. Figure 3 shows the S/N for detecting

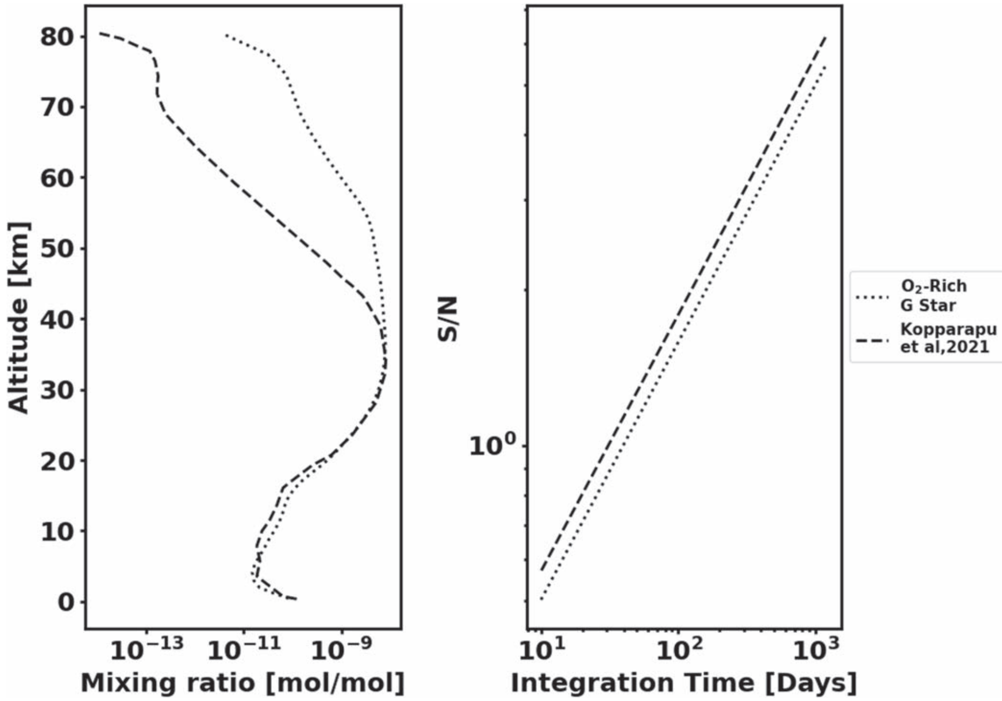

Figure 1. NO_2 vertical profile from Kopparapu et al. (2021) and our O_2-rich G-star planet (left). Signal-to-noise ratio (S/N) for a detection of NO_2 for both models assuming a LOIVOIR-type telescope with a 15 m diameter and only considering UV data, as in Kopparapu et al. (2021; right).

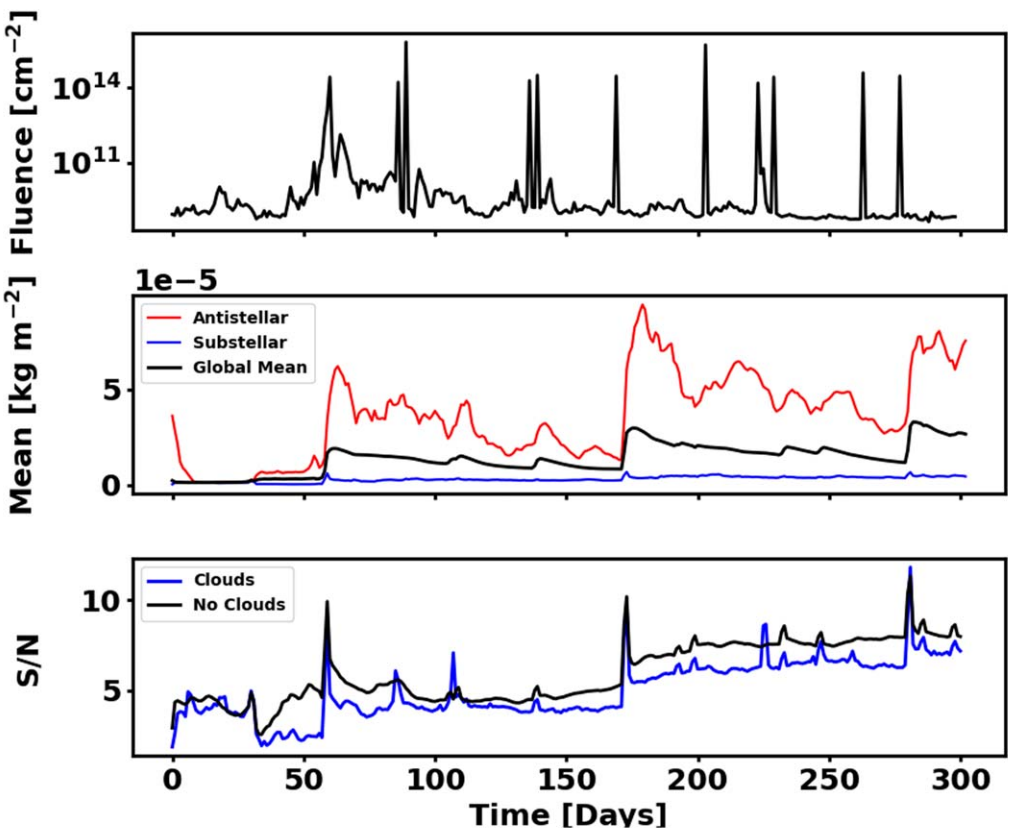

Figure 2. Time series of the proton fluence (stellar flares, top), global-mean NO_2 column (middle,black), NO_2 column at the antistellar point (middle, red), NO_2 column at the substellar point (middle, blue), and S/N of NO_2 including clouds in the calculation (bottom, blue) and excluding clouds (bottom, black) for an Earth-sized, oxygen-rich planet orbiting a K star that is 2 pc from Earth and observed at a phase of 45°.

changes in NO_2 as a function of integration period after the flare for two integration periods before the flare (5 and 10 days). The integration period before the flare is necessary to establish a baseline NO_2 value, and our results are not very sensitive to this integration time. We find that the optimal integration period after the flare is two days. This results from

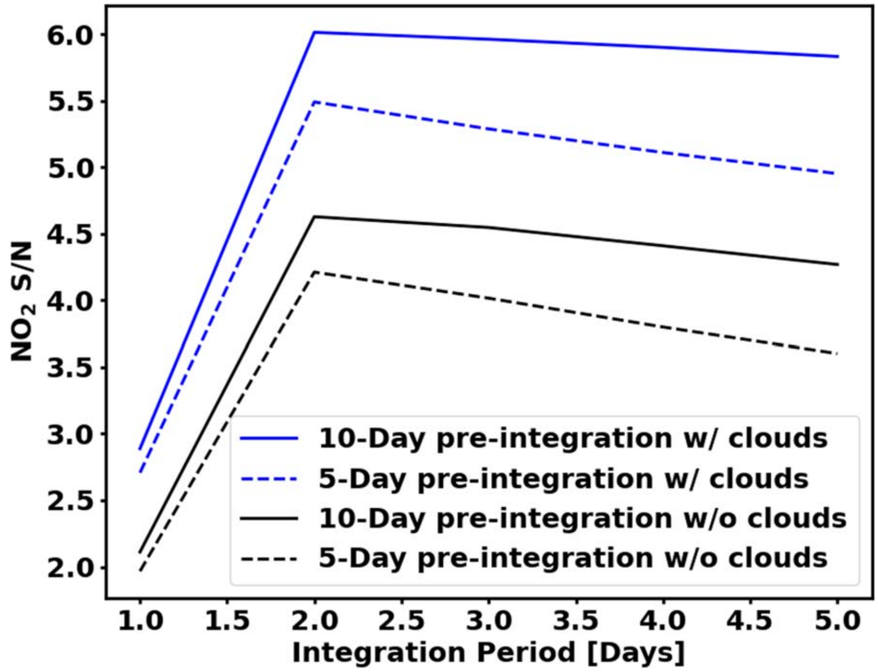

Figure 3. NO_2 S/N for the flare at days 58 in Figure 2 for different integration periods. We integrate the signal before the flare over 5 (dashed line) or 10 (solid line) days and after the flare has begun over a range of days (horizontal axis). We perform calculations both including clouds (blue) and without clouds (black).

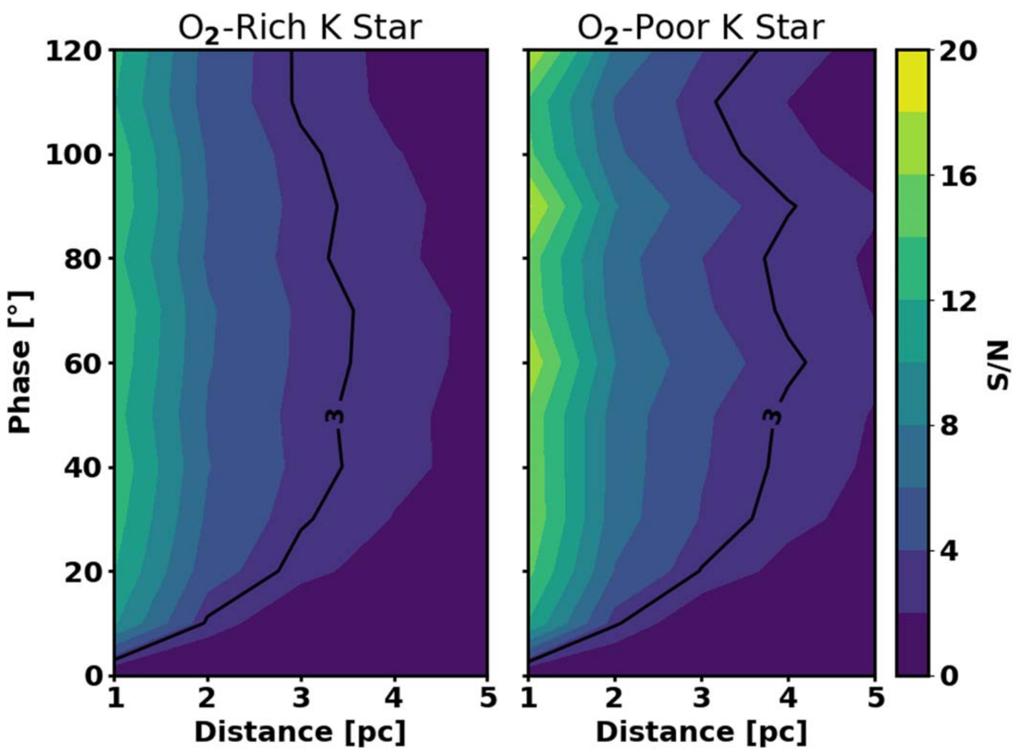

Figure 4. NO_2 S/N as a function of observing phase and distance for the O_2-rich and O_2-poor K-star scenarios. The black line marks a detectable S/N of 3. We use integration periods of 2 days after the flare and 10 days before the flare in this plot. These calculations include clouds.

competition between the NO_2 signal decaying quickly and more integration time leading to smaller noise. This is the case both for calculations including clouds and without clouds. Interestingly, the simulation with clouds yields a higher S/N for the observation because it has a smaller S/N before the flare. In both cases, two days after the flare and as many days as possible before the flare are the optimal integration periods.

Figure 4 shows the S/N as a function of orbital phase and distance for both the O_2-rich and O_2-poor K-star scenarios. Interestingly, the S/N is only weakly dependent on both O_2 level and phase. The weak phase dependence is due to a trade off between more reflected light at smaller phases and a larger NO_2 column on the night side (Figure 2), which is more visible at larger phases. We find that the NO_2 response to a large flare will be observable for K-star planets within about 3–4 pc regardless of their oxygen content.

4. Caveats

In this work we were limited to species that PSG includes, among which NO_2 was the most detectable. However, both NO and HNO_3 have absorption cross sections in the UV and visible at least as strong as NO_2 (Keller-Rudek et al. 2013), and would be useful molecules to investigate in the future.

NASA's IROUV direct-imaging space telescope is still in planning stages. We chose best-guess parameter options in PSG meant to correspond to how IROUV is currently being imagined (National Research Council 2021). Our conclusions might change if the IROUV specifications change, and our work may need to be repeated as the IROUV plan becomes more concrete.

The model data on which this paper is based assume stellar flares and proton events with fixed proton energy spectra derived from a series of specific solar observations (see also Segura et al. 2010 and Tilley et al. 2019). Proton flux and high-energy photon flux dependencies will be different depending on the stellar spectral type and the precise nature of the flaring event (Herbst et al. 2019; Hu et al. 2022). Significant vertical variations in the gaseous mean molecular densities and ion compositions suggest that sporadic distributions of proton energy spectra would lead to different cumulative photolytic/photochemical effects by virtue of deeper (or shallower) depositions of the incident charged particles.

The majority of studies using terrestrial photochemical models have considered the effects of flares on HO_x, NO_x, NO_y, and O_3, or species in N_2–O_2–H_2–CO_2-rich atmospheres. As future instruments will be observing planetary systems at various ages in their evolution, it is also important to perform similar assessments for flare-modulated compositions akin to early Earth by including reduced species. Such a study will necessitate using a more flexible GCM with a chemical framework capable of simulating the effects of ion chemistry on the formation of hydrocarbons and photochemical haze (Estrela & Valio 2018). It would also be instructive to simulate the observational consequences of stellar activity (including XUV irradiation and flares) on young planetary systems, as observing planetary-mass companions in the mid-infrared will be a high priority in the JWST GO program Cycles 1 and 2 (Hinkley et al. 2022; Miles et al. 2023). Vastly divergent pathways of atmospheric composition due to stochastic delivery/loss processes (Chen & Jacobson 2022) would also interface with the heightened flare frequencies and amplitudes during those epochs (Davenport et al. 2019). A study to explore a wide variety of initial planetary parameters would require the use of Monte Carlo calculations to test a range of flare rates on a range of timescales (e.g., Smith et al. 2004).

Our results do not allow us to determine whether flare-driven variations in NO_2 are more detectable for K-star planets than G-star planets because the K-star planets we simulated are tidally locked or because the stellar spectrum is different. More simulations would be required to determine the effect of rotation rate on the detectability of flare-driven variations in NO_2 for G-star planets.

Lastly (but perhaps most importantly), the precise effects of stellar flares on exoplanet atmospheres are complex and, to some degree, dependent on the particular model employed. Another GCM study using the Met Office unified model coupled with a chemical framework (Ridgway et al. 2023) reached somewhat different conclusions from Chen et al. (2021) and Tilley et al. (2019). They found that flares cause O_3 enhancement, as opposed to depletion, as UV-driven production offsets O_3 photolysis during the impulsive phase of the flaring events. These possibilities warrant model comparisons of observational predictions among different radiative transfer models, photochemical models, and climate models.

5. Conclusion

We find that the change in atmospheric NO_2 resulting from large flares should be detectable using NASAs future direct-imaging IROUV space observatory on Earth-like planets orbiting K stars within about 3–4 pc whether they are oxygen-rich ($\times 1$ present atmospheric level (PAL) of O_2) or oxygen-poor ($\times 10^{-3}$ PAL of O_2). This is an exciting result because it offers the opportunity to test the predictions of state-of-the-art Earth-system models employed in exoplanetary contexts including Community Earth System Model, the Met Office Unified Model, and others. Our work suggests that such a test will not be possible for planets orbiting G-stars. These conclusions should be further examined by studies with improved stellar flare, coronal mass ejection, magnetospheric transport, and atmospheric chemistry-climate models.

Acknowledgments

We thank Geronimo Villanueva for help using PSG. We thank Jacob Bean and Leslie Rogers for discussions about exoplanet observations. H.C. is supported by an appointment to the NASA Postdoctoral Program at Goddard Space Flight Center, administered by Oak Ridge Associated Universities under contract with NASA. This work was completed with resources provided by the University of Chicago Research Computing Center. This work was supported by the NASA Astrobiology Program grant No. 80NSSC18K0829, the UChicago Quad Grant, the UChicago Metcalf program and benefited from participation in the NASA Nexus for Exoplanet Systems Science research coordination network. This research made use of the open-source projects Jupyter (Kluyver et al. 2016), iPython (Pérez & Granger 2007), and matplotlib (Hunter 2007).

ORCID iDs

Howard Chen https://orcid.org/0000-0003-1995-1351
Jade Checlair https://orcid.org/0000-0001-8724-833X
Dorian S. Abbot https://orcid.org/0000-0001-8335-6560

References

Braam, M., Palmer, P. I., Decin, L., et al. 2022, MNRAS, 517, 2383
Checlair, J. H., Villanueva, G. L., Hayworth, B. P., et al. 2021, AJ, 161, 150
Chen, H., & Jacobson, S. A. 2022, E&PSL, 594, 117741
Chen, H., Wolf, E. T., Kopparapu, R., Domagal-Goldman, S., & Horton, D. E. 2018, ApJL, 868, L6
Chen, H., Wolf, E. T., Zhan, Z., & Horton, D. E. 2019, ApJ, 886, 16
Chen, H., Zhan, Z., Youngblood, A., et al. 2021, NatAs, 5, 298
Cooke, G., Marsh, D., Walsh, C., Rugheimer, S., & Villanueva, G. 2022, MNRAS, 518, 206
Davenport, J. R., Covey, K. R., Clarke, R. W., et al. 2019, ApJ, 871, 241
Estrela, R., & Valio, A. 2018, AsBio, 18, 1414
Fauchez, T. J., Turbet, M., Villanueva, G. L., et al. 2019, ApJ, 887, 194
Gao, P., Hu, R., Robinson, T. D., Li, C., & Yung, Y. L. 2015, ApJ, 806, 249
Grenfell, J., Gebauer, S., Godolt, M., et al. 2013, AsBio, 13, 415
Haqq-Misra, J., Kopparapu, R., Fauchez, T. J., et al. 2022, PSJ, 3, 60

Herbst, K., Papaioannou, A., Banjac, S., & Heber, B. 2019, A&A, 621, A67
Hinkley, S., Carter, A. L., Ray, S., et al. 2022, PASP, 134, 095003
Hu, J., Airapetian, V. S., Li, G., Zank, G., & Jin, M. 2022, SciA, 8, eabi9743
Hu, R., Seager, S., & Bains, W. 2012, ApJ, 761, 166
Hunter, J. D. 2007, CSE, 9, 90
Kaltenegger, L., & Sasselov, D. 2009, ApJ, 708, 1162
Keller-Rudek, H., Moortgat, G., Sander, R., & Sörensen, R. 2013, ESSD, 5, 365
Kinnison, D., Brasseur, G. P., Walters, S., et al. 2007, JGRD, 112, D20302
Kluyver, T., Ragan-Kelley, B., Pérez, F., et al. 2016, in Positioning and Power in Academic Publishing: Players, Agents and Agendas, ed. F. Loizides & B. Schmidt (Amsterdam: IOS Press), 90
Komacek, T. D., Fauchez, T. J., Wolf, E. T., & Abbot, D. S. 2020, ApJL, 888, L20
Kopparapu, R., Arney, G., Haqq-Misra, J., Lustig-Yaeger, J., & Villanueva, G. 2021, ApJ, 908, 164
Kozakis, T., Kaltenegger, L., & Hoard, D. 2018, ApJ, 862, 69
Miles, B. E., Biller, B. A., Patapis, P., et al. 2023, ApJL, 946, L6
National Research Council 2021, Pathways to Discovery in Astronomy and Astrophysics for the 2020 s (Washington, DC: The National Academies Press)
Pérez, F., & Granger, B. E. 2007, CSE, 9, 21
Ridgway, R. J., Zamyatina, M., Mayne, N. J., et al. 2023, MNRAS, 518, 2472
Segura, A., Kasting, J. F., Meadows, V., et al. 2005, AsBio, 5, 706
Segura, A., Walkowicz, L. M., Meadows, V., Kasting, J., & Hawley, S. 2010, AsBio, 10, 751
Smith, D. S., Scalo, J., & Wheeler, J. C. 2004, OLEB, 34, 513
Suissa, G., Wolf, E. T., kumar Kopparapu, R., et al. 2020, AJ, 160, 118
Tilley, M. A., Segura, A., Meadows, V., Hawley, S., & Davenport, J. 2019, AsBio, 19, 64
Tsai, S.-M., Lee, E. K., & Pierrehumbert, R. 2022, A&A, 664, A82
Villanueva, G. L., Smith, M. D., Protopapa, S., Faggi, S., & Mandell, A. M. 2018, JQSRT, 217, 86